Journal of Photochemistry and Photobiology A: Chemistry 215 (2010) 147–156

Contents lists available at ScienceDirect

Journal of Photochemistry and Photobiology A: Chemistry

journal homepage: www.elsevier.com/locate/jphotochem

Photocatalytic generation of silver nanoparticles and application to the antibacterial functionalization of textile fabrics

M. Messaoud[a], E. Chadeau[b], C. Brunon[c], T. Ballet[a], L. Rappenne[a], F. Roussel[d], D. Leonard[c], N. Oulahal[b], M. Langlet[a,*]

[a] Laboratoire des Matériaux et de Génie Physique, Grenoble Institute of Technology-Minatec, 3 Parvis Louis Néel, F-38016 Grenoble Cedex 1, France
[b] Université de Lyon, Université Lyon 1, Laboratoire de Recherche en Génie Industriel Alimentaire, LRGIA, E.A. no. 3733, Rue Henri de Boissieu, F-01000 Bourg en Bresse, France
[c] Université de Lyon, Université Lyon 1, Laboratoire des Sciences Analytiques (LSA), CNRS, UMR 5180, Bât. J. Raulin 5ème étage, F-69622 Villeurbanne Cedex, France
[d] Consortium des Moyens Technologiques Communs, Grenoble Institute of Technology, 1260 rue de la piscine, F-38402 Saint Martin d'Hères, France

ARTICLE INFO

Article history:
Received 2 April 2010
Received in revised form 2 July 2010
Accepted 2 August 2010
Available online 7 August 2010

Keywords:
Metallic silver
TiO_2
Nanoparticles
Textile
Photocatalysis
Antibacterial activity

ABSTRACT

An all-inorganic protocol, entirely based on wet chemistry methods, has been studied to form nano-sized Ag metallic particles in solution. Liquid suspensions of anatase TiO_2 nanocrystallites have first been prepared through a sol–gel route. Silver nanoparticles (NPs) have then been generated through the photocatalytic reduction of a silver salt, diluted in TiO_2 liquid suspensions, and exposed to UV light, which results in the formation of a mixed Ag–TiO_2 suspension. Mechanisms occurring in solutions during the metallization step and a post-metallization ageing period have been studied by UV/vis spectroscopy. Chemico-structural and morphological properties of resulting silver NPs have been studied by transmission electron microscopy, scanning electron microscopy, and X-ray photoelectron spectroscopy. Ag–TiO_2 suspensions have then been impregnated on cotton-based textile samples and the antibacterial activity of so-functionalized textiles has been studied with respect to *E. coli* and *L. innocua* bacteria. It is shown that, while TiO_2 NPs attached to textile fibres have no antibacterial activity, functionalized textiles exhibit a strong antibacterial activity due to Ag NPs, and this activity can be reached for a large range of impregnated silver amounts.

1. Introduction

In recent years, the antibacterial or antimicrobial finishing of fibres and fabrics used in various environments has attracted much attention [1–4]. In this approach, most finished textile materials currently introduced in hospitals and food industries are used to protect wearers against the spread of nosocomial infections, inhibit the formation of pathogen biofilms, and remove the infection sources. In general, antibacterial properties can be imparted to the textile materials by chemically or physically incorporating functional agents onto fibres of fabrics. Researchers are now focusing on durable and environmentally friendly agents with much interest in finding ways to formulate in cost-effective manner new types of safe antibacterial agents. Previous studies have shown that active agents in the form of nanoparticles (NPs) can be envisaged as new antibacterial materials. Recently, Klabunde and co-workers demonstrated that highly reactive metallic oxide NPs exhibited good biocidal action against both Gram-positive and Gram-negative bacteria [5]. Thus, the formulation of nano-sized inorganic particles displaying unique physical and chemical properties opens the possibility of a new generation of antibacterial materials [6]. New studies of efficient active agents are all the more a topical subject, as several pathogenic bacteria have shown enhanced resistance against various antibiotics.

Silver-based compounds, being biocompatible at effective concentrations, are particularly investigated as antibacterial agents against micro-organisms when in the form of non-agglomerated and well dispersed NPs [7–11]. On the one hand, the antibacterial activity of silver cations is well known and has been studied in details [12]. On the other hand, beside inherent chemical, physical, and optical properties arising from their very small size, Ag metallic NPs have recently shown a promising potential as antibacterial or antimicrobial agents [13]. Many techniques well covered in literature have been developed to prepare metallic silver NPs. For example, such NPs can be synthesized through γ-radiation [14], laser ablation [15], electrochemical [16], chemical [17], photochemical [18] methods, and else. Because of their cost-effectiveness, wet chemistry (chemical or photochemical) methods are particularly studied. In these approaches, silver NPs are formed in solution and then dispersed on functional supports. Such chemical and photochemical procedures often involve multiple organic chemicals, used as reductive, capping, and/or surfactant agents, and

* Corresponding author. Tel.: +33 456529342.
E-mail address: Michel.Langlet@grenoble-inp.fr (M. Langlet).

1010-6030/$ – see front matter © 2010 Elsevier B.V. All rights reserved.
doi:10.1016/j.jphotochem.2010.08.003

intended to control the mean size, size distribution, and stability of silver NPs in solution. For instance, the use of $NaBH_4$ or citrate additives is very well documented in the literature [19–21]. However, organic chemicals can alter or shield the function of metallic NPs. In clothing applications, they can also provoke biological hazards when contacted with human skin [7]. Finally, aforementioned chemical and photochemical procedures involve quite tedious multi-step processes, which are not necessarily compatible with industrial aspects [22].

In this work, an all-inorganic two-step protocol, entirely based on wet chemistry methods, has been studied to form nano-sized Ag metallic particles in solution. Liquid suspensions of anatase TiO_2 nanocrystallites have first been prepared through a sol–gel route. Silver NPs have then been generated through the photocatalytic reduction of silver nitrate diluted in TiO_2 liquid suspensions exposed to UV light, which results in mixed Ag–TiO_2 suspensions. In this paper, we firstly focus on the formation of silver NPs and their optimization with respect to the metallization yield as well as their mean size, size distribution, and stability in solution. Size effects are a particular matter of interest because it has been shown that interactions of silver NPs with bacteria are dependent on the size and shape of the nanoparticles [23]. Then, the antibacterial action of metallic Ag NPs impregnated on textile materials through a pad-coating procedure is presented. Antibacterial activity assessments have been performed using Gram-negative *E. coli* and Gram-positive *L. innocua* as model bacteria.

2. Experimental

2.1. Preparation of TiO_2 liquid suspensions

Titanium oxide liquid suspensions were prepared using a sol–gel route, as schematically illustrated in Fig. 1a. In a first preparation step, a polymeric sol (PS) was formed by mixing tetraisopropyl orthotitanate (TIPT) with deionised water, hydrochloric acid (HCl), and absolute ethanol as a solvent [24]. The TIPT concentration in the sol was 0.4 M, and the TIPT/H_2O/HCl molar composition was 1/0.82/0.13. The sol was aged at room temperature for 2 days before use in a second preparation step. In this second step, the PS sol was first diluted in an excess of deionised water (H_2O/TIPT molar ratio of 90) and then autoclaved at 130 °C for 6 h. Autoclaving yielded the crystallization of anatase TiO_2 NPs in the liquid phase. An exchange procedure was then performed in order to remove water from the sol and form a crystalline suspension (CS) in absolute ethanol. The final TiO_2 concentration in ethanol was 0.24 M. For more data, the whole procedure has been described in a previous paper [25]. The final sol was composed of TiO_2 nanocrystallites of about 6 nm in diameter, which were aggregated in the form of polycrystalline grains of 50–100 nm in size. Previous works showed that both PS and CS preparation conditions gave rise to very stable sols, which indicated that no gelation took place in PS sols, while no significant particle aggregation occurred in CS sols. Consequently, these sols could be used for several weeks in reproducible conditions.

2.2. Photo-generation of silver nanoparticles in solution

The process yielding the formation of Ag NPs in solution is schematically represented in Fig. 1b. Silver nitrate ($AgNO_3$), used as Ag precursor, was first diluted at various concentrations in absolute ethanol and the mixture was then added to a CS previously diluted in absolute ethanol at various concentrations. $AgNO_3$ and TiO_2 concentrations in resulting solutions were varied in the $[0.037 \times 10^{-3}–5 \times 10^{-3}$ M] and $[0.024 \times 10^{-3}–2.4 \times 10^{-3}$ M] ranges, respectively. These solutions were magnetically stirred for 15 min at 500 rpm, then poured into a glass vessel and exposed to radiation arising from three UVA lamps (PLS 11W from Philips) essentially emitting at 365 nm wavelength (negligible UVB/UVC emission). UV exposure experiments were performed for various durations, ranging up to 1 h, in a climatic cabinet regulated at a 20 °C temperature and 40% relative humidity. Constant agitation of the solution was insured over UV exposure using a magnetic stirrer rotated at 500 rpm. As will be discussed hereafter, this procedure resulted in mixed Ag–TiO_2 liquid suspensions.

2.3. Substrates and antibacterial textile finishing

Silicon wafers were used as supports to routinely study some characteristics of NPs formed through the aforementioned procedure. For that purpose, 5–10 droplets of derived liquid suspensions were spread on the substrate surface in order to deposit a sufficient quantity of matter to be analyzed. Besides, antibacterial tests were performed on 65% cotton–35% polyester textiles, furnished by an industrial society. More precise data on these textiles cannot be furnished for confidentiality reasons. The impregnation procedure

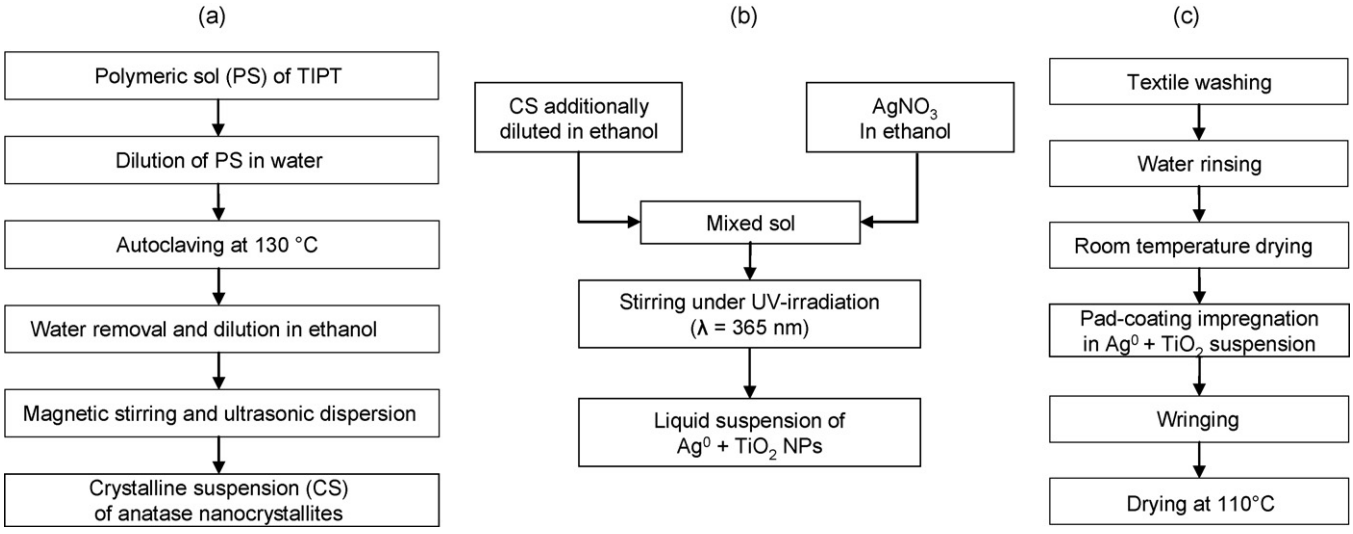

Fig. 1. Schematic illustration of the process yielding antibacterial functionalization of textile fabrics: preparation of a TiO_2 crystalline suspension through sol–gel route (a), preparation of an Ag–TiO_2 mixed suspension through a photocatalytic reduction mechanism (b), and impregnation of the textile within an Ag–TiO_2 mixed suspension (c).

of textile samples with Ag–TiO_2 liquid suspensions is schematically represented in Fig. 1c. Household washing was preliminary performed at 40 °C using the ECE laundering powder (1 g/L) in order to eliminate dusts and impurities. Textiles were then rinsed 3 times with water, and finally dried at ambient temperature. Textile samples of 30 cm × 7 cm dimensions were impregnated in Ag–TiO_2 liquid suspensions of various compositions through a pad-coating procedure with an immersion speed of 5 m/min. The finished textile was then wrung twice between a plane support and an upper squeezing roll to remove the excess of liquid suspension and fix the remaining finish on the textile. The textile was finally dried at 110 °C for 10 min to totally eliminate the solvent (ethanol).

2.4. Characterization methods

Modifications occurring in the solutions exposed to UV light were analyzed by UV/vis spectroscopy, in a 200–500 nm spectral range, using a Jasco V-530 spectrophotometer. Over UV exposure, small solution aliquots were periodically withdrawn for spectral measurement. Morphological and chemical characterizations were generally realized on NPs deposited on silicon substrates. Nanoparticle imaging was performed using a ZEISS Ultra 55 field emission gun scanning electron microscope (FEG-SEM) operated at 20 kV. NPs counting was realized from FEG-SEM images using an Image-Pro Plus V4 software. NPs dispersed on textile fibres were also imaged using a controlled pressure FEG-SEM (Zeiss Ultra 55 VP) with a chamber pressure of 100 Pa. Surface chemical analysis of NPs was performed by X-ray photoelectron spectroscopy (XPS) using a PHI Quantera SXM instrument (physical electronics) equipped with a 180° hemispherical electron energy analyzer and a monochromatized Al Kα (1486.6 eV) source operated at 15 kV and 4 mA. The analysis spot had a diameter of 200 μm and the detection angle relative to the substrate surface was 45°. In such conditions, the probed depth was estimated to be around 3 nm. Samples were analyzed with dual-beam charge neutralisation and the C–C/C–H component of C_{1s} peak was adjusted to 285 eV. The so-called modified Auger parameter was calculated from the sum of the $Ag_{3d5/2}$ photoelectron binding energy and of the $Ag_{M4N45N45}$ Auger electron kinetic energy. Structural characterizations were performed thanks to transmission electron microscopy (TEM) observations. For that purpose, NPs were dispersed on a carbon grid and then studied using a JEOL-2010 LaB6 TEM operated at 200 keV. Fast Fourier transform (FFT) was performed on several high resolution TEM (HRTEM) images to identify the simultaneous presence of Ag and TiO_2 nanoparticles.

2.5. Bacterial strains and determination of the antibacterial activity

Determination of the antibacterial activity was focused on the Gram-negative bacteria *E. coli* (XL1-blue) and the Gram-positive bacteria *L. innocua*. The latter kind of strains were isolated from a dairy environment. All strains were stored at −20 °C in brain heart infusion (BHI) media added with 15 vol% glycerol. The whole protocol, which is adapted from the ISO 20743-2005 (Anon., 2005) standard for the determination of the antibacterial activity on textiles, has been detailed elsewhere [26]. Briefly, after different incubation times at 30 °C, i.e. different contact durations of bacteria at the surface of textile fibres, bacterial cells were removed from the textile and the number of cells forming colony on trypticase soy agar (TSA) was counted and expressed relatively to the weight of the textile sample in log (CFU/g) units. Bacterial evolution kinetics were studied by plotting log (CFU/g) as a function of the incubation time and the antibacterial activity (A) of the finishing treatment was calculated after 24 h of incubation according to $A = (C^{24} - C^0) - (T^{24} - T^0)$, where C and T represent the numbers of bacteria counted after removal from control (untreated) and treated textiles, respectively, and "24" and "0" account for times of incubation (in hours) for each condition. According to the ISO 20743-2005 standard, the finishing treatment is considered to be active when the antibacterial activity exceeds a value of 2.

3. Results and discussion

3.1. UV/vis spectral features

The UV–vis spectrum illustrated in Fig. 2a shows that silver nitrate only absorbs light at around 215 nm and does not show any absorption in the UVA range, i.e. the emission range of lamps used in the present work. In these conditions, any direct photochemical (photolytic) reduction of Ag^+ cations, which would eventually produce Ag NPs, cannot be expected under UVA light. In contrast, spectra of Fig. 2b–f shows that increasing the relative amount of TiO_2 NPs in the solution promotes the appearance and growth of a second UV absorption band at greater wavelengths and a progressive absorption overlap in the emission range of our lamps. It is well known that, when exposed to UV radiation ($\lambda < 380$ nm), titanium oxide (preferentially in its anatase polymorphic form) absorbs light and exhibits photocatalytic properties induced by electron (e^-)/hole (h^+) pairs photo-generated in the TiO_2 particles [27]. Photo-generated electrons can in particular induce a reduction of cations adsorbed at the TiO_2 surface [28]. This mechanism has been used in the present work to promote the photo-reduction of $AgNO_3$ into Ag NPs. The anodic process associated to this reduction mechanism is the oxidation of a sacrificial oxidable reactant by valence band photo-holes. In this work, ethanol employed as a dilution medium of $AgNO_3$ salt and TiO_2 particles, was also used as an oxidable reactant. This hole-scavenger, which favours a better photo-generated charge carrier separation, is expected to promote a more efficient photo-reduction and to enhance the rate of metallization leading to Ag NPs.

It is known that metallic silver NPs exhibit an intense absorption band due to surface plasmon resonance (SPR) effects. According to Mie theory, the SPR arises from interactions of small metallic particles with an external electromagnetic field, induced by light, resulting in a coherent oscillation of the conduction (free) electrons at the surface [29,30]. During UV exposure, we observed that $AgNO_3/TiO_2$ ethanolic solutions gradually turned from colorless to yellow or dark yellow. This coloration is attributed to a growing absorption at short wavelengths of the visible spectrum, arising from the progressive appearance of plasmon effects, and it provides a first evidence of the photo-metallization reaction occurring

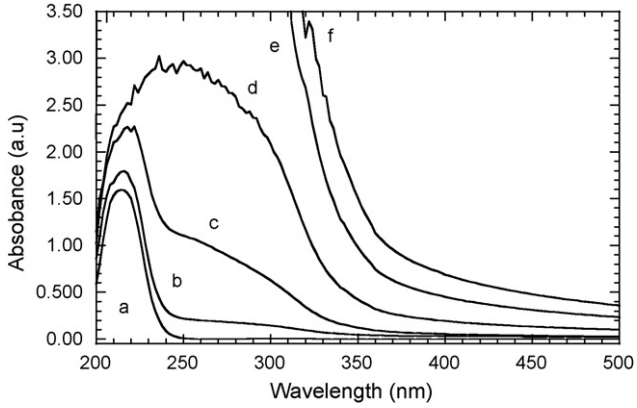

Fig. 2. UV–vis spectra of $AgNO_3$ ($C = 0.5 \times 10^{-3}$ M) diluted in pure ethanol (a) and in a CS suspension with a TiO_2 concentration of 0.25×10^{-4} (b), 1.2×10^{-4} (c), 2.4×10^{-4} (d), 1.2×10^{-3} (e), and 2.4×10^{-3} M (f).

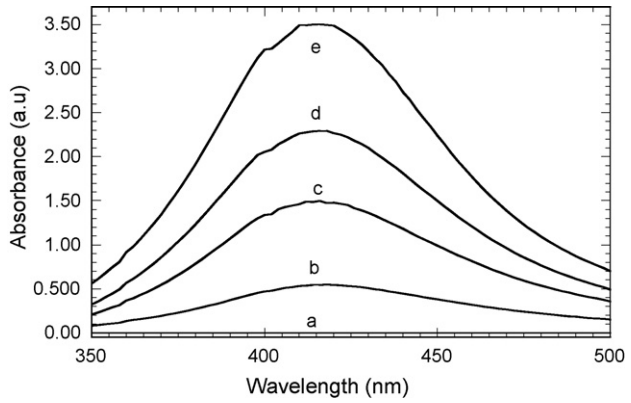

Fig. 3. SPR band at 420 nm for a mixed solution, composed of $AgNO_3$ ($C = 0.5 \times 10^{-3}$ M) and TiO_2 ($C = 1.2 \times 10^{-3}$ M), and exposed to UV light for 0 (a), 5 (b), 15 (c), 30 (d), and 60 min (e). Spectra have been normalized to the spectrum of the solution before UV exposure.

in the solution. Typical absorption spectra of a solution exposed to UV light for various durations are presented in Fig. 3. For more clarity, spectra presented in this figure have been normalized to the spectrum of the solution before UV exposure, i.e. $AgNO_3$ and TiO_2 absorption bands illustrated in Fig. 2 have been subtracted from the UV/vis spectra of irradiated solutions. These normalized spectra illustrate the appearance and growth of a well defined absorption band located at around 420 nm. The more or less rapid development of such a band under UV exposure was observed for all the solutions studied here. The location of this band is coherent with SPR effects induced by metallic silver NPs [31,32]. In the present work, intensity of the 420 nm band deduced from normalized spectra has been used to study the photo-metallization reaction occurring in solution under UV exposure.

3.2. Photo-metallization kinetics

Fig. 4 shows intensity variations of the normalized SPR band at 420 nm over UV exposure for mixed solutions of 0.5×10^{-3} M $AgNO_3$ concentration and various TiO_2 concentrations. For a same amount of silver precursor in the solution, it is observed that the formation of metallic silver NPs, i.e. intensity growth of the SPR band, strongly depends on the TiO_2 amount. On the one hand, increasing the TiO_2 concentration from 2.4×10^{-5} to 1.2×10^{-3} M (Fig. 4a–c) yields an increasing metallization rate. This rate is generally rapid over the first UV exposure stages, after what it slows down or even shows a plateau. Beneficial influence of the TiO_2 amount firstly suggests an activation of the photo-reduction reaction induced by the photocatalytic activity of TiO_2 nanocrystallites. On the other hand, Fig. 4c and d shows that further increase in the TiO_2 amount does not improve and even reduces the metallization rate. Overall trends illustrated in Fig. 4 suggest, therefore, a competition between photocatalytic activation and UVA light absorption arising from TiO_2 NPs. Above a certain TiO_2 concentration threshold, it is likely that UVA absorption by TiO_2 NPs predominates, which reduces penetration of light within the irradiated solution and thus decreases the metallization yield. Beside, it should be noted that kinetic behaviours illustrated in Fig. 4 do not only depict metallization features but also the aggregation and subsequent decantation of photo-generated metallic particles. Accordingly, for a weak TiO_2 concentration of 2.4×10^{-5} M, particles were visually observed to rapidly decant during UV irradiation, which could also explain why the SPR band illustrated in Fig. 4a for this solution did not significantly increase in intensity over UV exposure. These decantation features will be discussed below. Finally, data illustrated in Fig. 4 can also depict a competition between metallization advancement and UVA light absorption by Ag NPs formed in solution. Indeed, Fig. 3 shows that the SPR band of Ag NPs partly overlaps the emission range of our UVA lamps. Thus, while Ag particles are progressively formed in solution, this latter is expected to absorb more and more UVA light, yielding a decrease in light penetration and a metallization yield reduction over UV exposure.

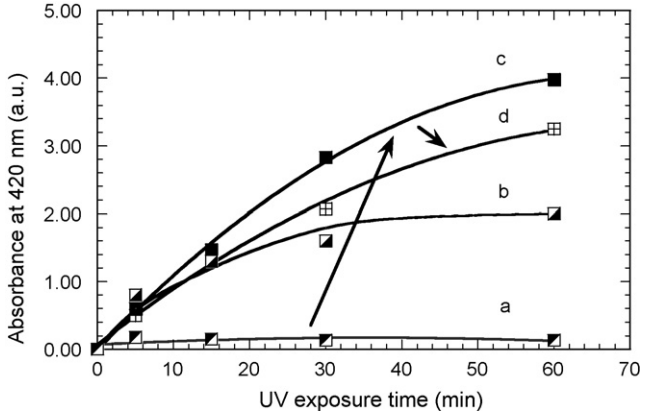

Fig. 4. Intensity variations of the normalized 420 nm SPR band over UV exposure for mixed solutions with 0.5×10^{-3} M $AgNO_3$ concentration and TiO_2 concentrations of 0.24×10^{-4} (a), 1.2×10^{-4} (b), 1.2×10^{-3} (c) and 2.4×10^{-3} M (d).

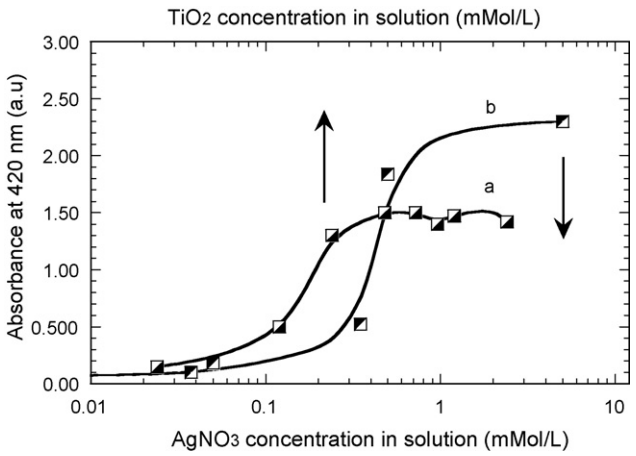

Fig. 5. Intensity of the normalized 420 nm SPR band measured after 15 min UV exposure for solutions of various TiO_2 concentrations ($AgNO_3$ concentration of 0.5×10^{-3} M) (a) and various $AgNO_3$ concentrations (TiO_2 concentration of 1.2×10^{-3} M) (b).

Previously drawn conclusions are globally confirmed by data illustrated in Fig. 5, which depicts intensity variations of the normalized SPR band measured after 15 min UV exposure as a function of the $AgNO_3$ concentration (TiO_2 concentration) for a fixed TiO_2 concentration ($AgNO_3$ concentration) in the solution. This figure shows that below $AgNO_3$ and TiO_2 concentration thresholds of around 0.1×10^{-3} M, the metallization proceeds extremely slowly. The metallization rate is observed to strongly increase when further increasing the concentration of $AgNO_3$ and TiO_2 up to around 0.5×10^{-3} M. An autocatalytic reduction mechanism can eventually participate in the sudden acceleration of the metallization reaction when increasing the $AgNO_3$ concentration, i.e. initially formed Ag NPs can in turn participate in the photo-reduction mechanism owing to their photochemical activity [33]. Finally, Fig. 5 shows that increasing the reactant concentrations above around 0.5×10^{-3} M does not yield significant improvement in the metallization rate, which is attributed to a predominant UV light absorption by Ag and TiO_2 NPs in the solution, i.e. a reduction of light penetration in the solution exposed to UV.

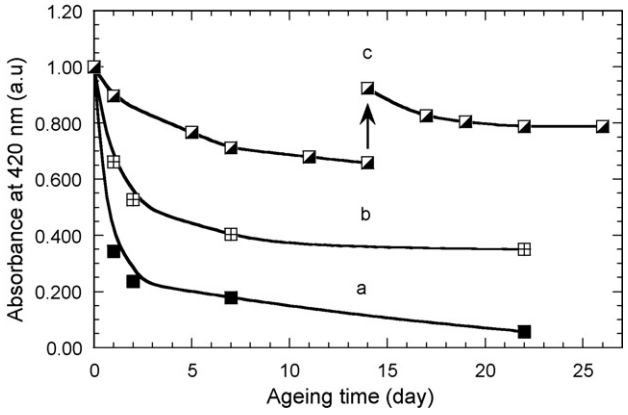

Fig. 6. Stability of Ag NPs in solution over ageing, as deduced from the 420 nm SPR band intensity variations, for solutions previously exposed to UV light for 60 min with an $AgNO_3$ concentration of 0.5×10^{-3} M and TiO_2 concentrations of 2.4×10^{-4} (a), 1.2×10^{-3} (b), and 2.4×10^{-3} M (c). Spectra have been normalized to those measured before ageing. The arrow shows the instant where magnetic stirring has been performed.

3.3. Stability of Ag NPs in solution

From an applicative point of view, a reasonable stability over ageing of NPs formed in solution, i.e. prevention of their decantation, is an important feature to be studied since it determines the reproducible use of our suspensions in the long-term. On the one hand, solutions with high Ag concentrations did not exhibit good stability over ageing. On the other hand, the presence of TiO_2 NPs was observed to impact the solution stability over ageing. As already mentioned, and illustrated in Fig. 4a, for a fixed $AgNO_3$ concentration of 0.5×10^{-3} M, a solution with a very weak TiO_2 concentration (0.24×10^{-4} M) rapidly decants even during UV exposure. Fig. 6 illustrates variations of the SPR band intensity over ageing for three solutions previously exposed to UV light for 60 min with a fixed $AgNO_3$ concentration of 0.5×10^{-3} M and TiO_2 concentrations ranging from 2.4×10^{-4} to 2.4×10^{-3} M. For comparison purpose, SPR band intensities have been normalized to the value measured before ageing. The solution with the weakest TiO_2 amount was visually observed to rapidly decant over ageing, and this decantation yielded a rapid drop and quasi-extinction of the SPR band (Fig. 6a), i.e. a nearly total decantation of Ag NPs. Fig. 6b and c shows that increasing the TiO_2 amount strongly reduces the intensity drop of the SPR band. Ageing for 2 weeks solutions with TiO_2 concentrations of 1.2×10^{-3} and 2.4×10^{-3} M yielded a reduction of the SPR band intensity by 60% and 30%, respectively, which depicted a reduced decantation of silver NPs. No additional decantation was observed with further ageing of these solutions, which were observed to remain naturally stable for several additional weeks. Fig. 6c also shows that, for a solution with the greatest TiO_2 concentration studied here, a simple magnetic stirring for 10 min is sufficient to recover the initial SPR band intensity, i.e. to regenerate the solution. These data indicate that, above a certain threshold value of the $TiO_2/AgNO_3$ ratio, resulting Ag–TiO_2 suspensions can be efficiently stabilized on the long-term. In other words, TiO_2 NPs not only act as photo-reductive reactants, but also play a role of stabilizing agents, similarly to what is commonly reported in the literature for organic stabilizers used in chemical or photochemical reduction procedures. As previously mentioned, pure TiO_2 CS sols exhibit good stability on the long-term, which is attributed to electrostatic repulsion effects between positively charged TiO_2 NPs formed in acidic solution [25]. It is supposed that such electrostatic repulsion effects can also contribute in the stabilisation of Ag NPs, provided that the initial $TiO_2/AgNO_3$ molar ratio in the solution is close to an optimal threshold value. For conditions illustrated in Fig. 6, we can infer a threshold value corresponding to a $TiO_2/AgNO_3$ molar ratio of around 5. According to metallization and stability features illustrated in Figs. 3–6, following parts of this work will be focused on optimized Ag–TiO_2 suspensions arising from solutions exposed to UV light for 60 min with 0.5×10^{-3} M $AgNO_3$ and 2.4×10^{-3} M TiO_2 concentrations.

3.4. Structural and morphological features

Fig. 7 illustrates TEM images of particles deposited on a carbon grid from the optimized Ag–TiO_2 suspension. Owing to weight contrast effects, silver particles are expected to produce darker features than TiO_2 ones. Darker spots observed in Fig. 7 are thus attributed to metallic silver particles while grey spots correspond to TiO_2 rich areas. From the analysis of several low magnification TEM and high magnification HRTEM images, it was deduced that most silver particles had a diameter ranging between 2 and 15 nm. Besides, lines observed in HRTEM images of Fig. 7b and c correspond to reticular planes, which indicate the crystalline state of silver particles. It is illustrated in Fig. 7d, which shows the diffraction pattern derived from a FFT of the HRTEM image displayed in Fig. 7c. An indexation of this pattern depicts a particle orientated along the [0 1 1] zone axis of the centred face cubic (CFC) structure of metallic silver, and white spots observed in the pattern are assigned to three reticular plane families of this structure, i.e. (−1 1 −1), (1 1 −1), and (2 0 0) planes. The analysis of various patterns allowed a systematic assignment of reticular planes to the CFC structure of metallic silver. These observations, in agreement with plasmon features illustrated in Fig. 3, prove the metallic state of silver NPs formed through our photocatalytic reduction process. TiO_2 particles in the anatase structure were also clearly put in evidence from FFTs of various HRTEM images (not illustrated here).

Fig. 8a shows a typical FEG-SEM image of a silicon substrate covered with particles derived from the optimized Ag–TiO_2 suspension. Owing to weight contrast between silver particles and TiO_2 ones (together with the silicon substrate), white spots observed in this image are assigned to silver nanoparticles. It is observed that so-formed particles do not continuously coat the substrate but are rather homogeneously dispersed on its surface. A small number of large particles can be evidenced in this figure which were not observed by TEM. However, as illustrated in the insert of Fig. 8a, image counting performed from FEG-SEM inspections confirmed the rather narrow size distribution of Ag NPs deduced from TEM investigations, since 90% of silver NPs presented diameters ranging from 2 to 15 nm. It is worthy to mention that similarly small Ag particles have been reported to be very effective against *E. coli* bacteria [12,34]. Actually, small size effects have been reported to be at the origin of an enhanced reactivity of such nanoparticles [12,35].

3.5. Metallization degree of silver particles

Fig. 9 shows the typical Ag_{3d} doublet spectrum measured on a silicon substrate coated with an Ag–TiO_2 suspension. $Ag_{3d5/2}$ and $Ag_{3d3/2}$ components of the doublet are depicted by binding energies of around 368 and 374 eV, respectively. This doublet illustrates the presence of silver particles at the substrate surface. Energy positions of XPS peaks can, in principle, provide information on the oxidation degree of noble metals. However, in the case of silver, data of the literature show that $Ag_{3d5/2}$ peak energies of metallic silver (Ag) and silver in its most probable oxidation state (Ag_2O) lie in the very narrow range of 367.6–368.3 eV [36], which does not allow drawing reliable conclusions on the silver oxidation degree. For this reason, the modified Auger parameter was studied. As previously mentioned, this parameter relies on the sum of the $Ag_{3d5/2}$ photoelectron binding energy and of the $Ag_{M4N45N45}$ Auger electron kinetic energy. Auger parameter values of around 725.8–726 eV

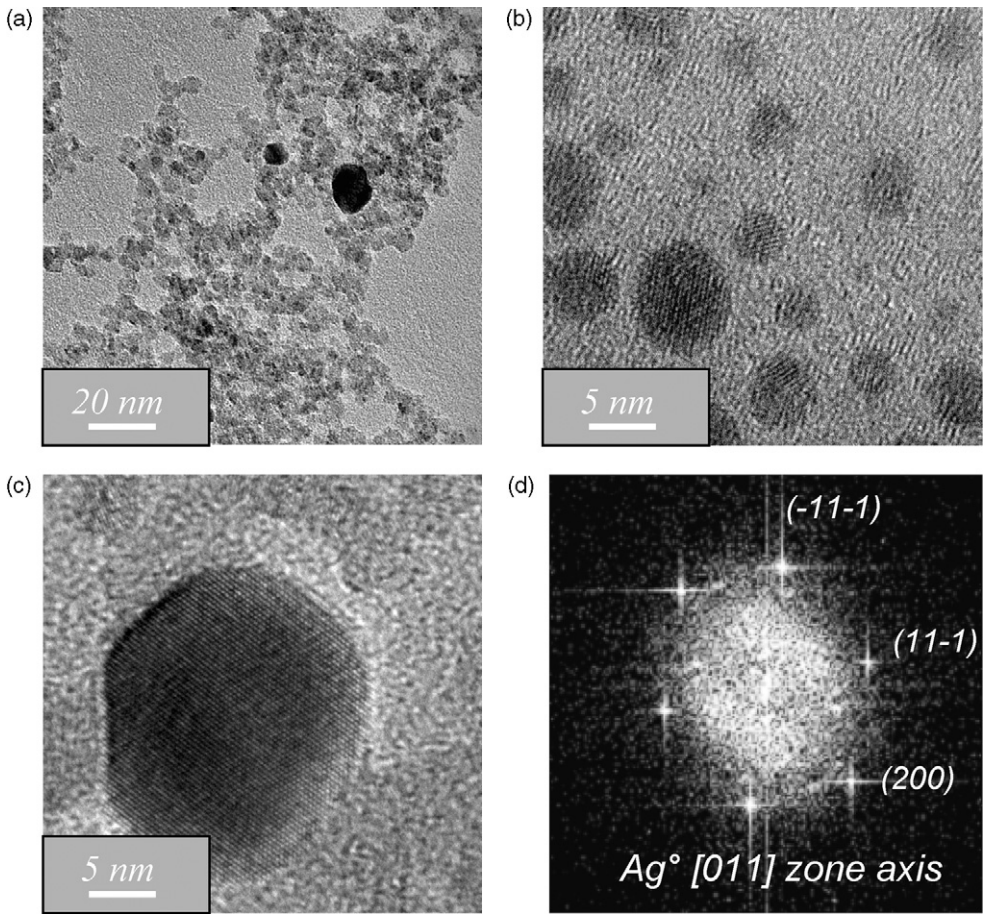

Fig. 7. Low magnification TEM image of silver (dark contrast) and TiO_2 (grey contrast) particles (a), and HRTEM images of silver NPs (b and c). Fig. 6d illustrates an electron diffraction pattern derived from FFT of the HRTEM image displayed in Fig. 6c.

were reproducibly measured on several samples, which demonstrated the accurate determination of this parameter. Literature data show that silver in its Ag_2O or (less probable) AgO oxidized forms yields an Auger parameter in the 724–724.8 eV range, while metallic silver yields an Auger parameter in the 726–726.3 eV range [37–39]. Thus, values measured on our samples appear to be rather close to those mentioned for metallic silver. However, since our Auger parameter values are slightly weaker than those mentioned for metallic silver, it suggests a slight oxidation degree, which probably depicts the formation of an oxide layer at the surface of metallic NPs. Thus, XPS data support conclusions previously drawn from UV/vis spectroscopy and TEM characterizations showing that metallic particles have been formed in solution. From these different observations, we conclude that photo-reduction of $AgNO_3$, i.e.

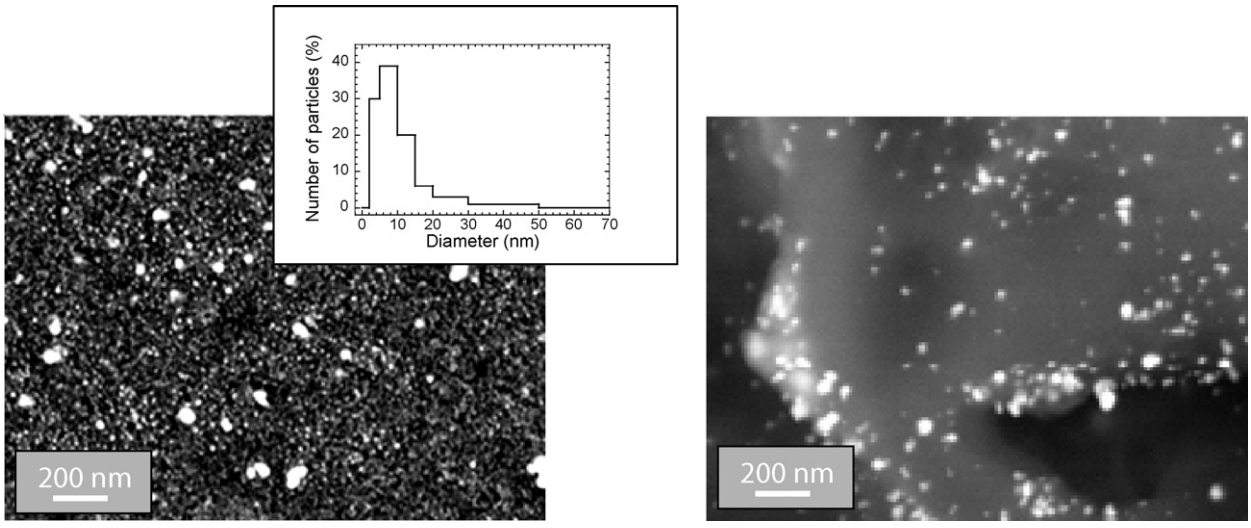

Fig. 8. FEG-SEM images of silver NPs (white spots) dispersed on a silicon wafer (a) and impregnated on a cotton-based textile (b). The insert shows the size distribution of silver NPs illustrated in Fig. 7a.

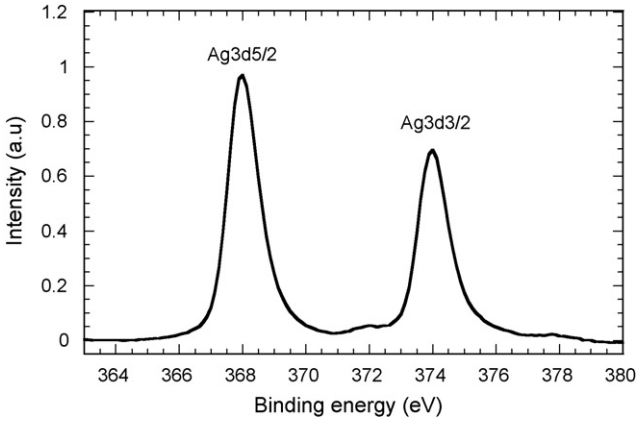

Fig. 9. XPS spectrum of the Ag_{3d} doublet measured for silver NPs dispersed on a silicon wafer. The spectrum has been normalized to intensity of the $Ag_{3d5/2}$ peak.

the photo-metallization reaction, has probably gone to completion in present conditions.

3.6. Textile impregnation

The FEG-SEM image of a textile sample impregnated with an Ag–TiO_2 suspension is illustrated in Fig. 8b. This image shows that, similarly to what occurs on silicon, silver particles (white spots) do not continuously coat the textile fibres but are rather uniformly dispersed at the fibre surfaces. The size of Ag particles illustrated in Fig. 8b is rather similar to that illustrated in Fig. 8a for a silicon substrate. However, smallest particles appearing in Fig. 8a cannot be appreciated in Fig. 8b, which is probably due to some sensitivity limitations of the controlled pressure FEG-SEM used to characterize textile samples. Energy dispersive X-ray (EDX) analyses performed on such samples depicted a Ti/Ag atomic ratio of around 5 (not illustrated here) which suggested that, in our textile impregnation procedure, TiO_2 and Ag NPs were deposited au prorate of the TiO_2 and Ag concentrations in the mixed solution. To provide a first insight in the yield of our whole process, weight measurements were performed on five textile samples, before and after the impregnation/wringing procedure (without drying at 110 °C). In that way, pick-up of the finishing solution normalized to the bare textile weight could be estimated to be 67 ± 4 wt%. From this average value and taking into account the weight percentage of Ag in the solution (assuming a total photo-metalization process according to previously discussed data), we could finally estimate the amount of impregnated silver NPs per surface unit of textile to be around 1.16×10^{-2} g/m^2.

3.7. Antibacterial tests

To assess the antibacterial efficiency of our finished textile fabrics, Ag–TiO_2 suspensions were first diluted in absolute ethanol by a factor 1–10. Textile samples were then impregnated through a pad-coating procedure within resulting suspensions and antibacterial tests were finally performed against Gram-negative *E. coli* and Gram-positive *L. innocua* bacteria. Preliminary tests indicated that control textiles, as well as textiles impregnated with only TiO_2, did not exhibit any antibacterial effect against *E. coli*. These features are globally illustrated in Fig. 10, which typically shows Petri dishes after a 24 h incubation time of *E. coli* at the surface of textile supports. A dense population of bacterial colonies appears after incubation on a control textile (Fig. 10a) and textile only impregnated with TiO_2 particles (Fig. 10b). On the one hand, these observations suggest that textile fabrics, especially those made from natural fibres (cotton-based), can provide excellent conditions

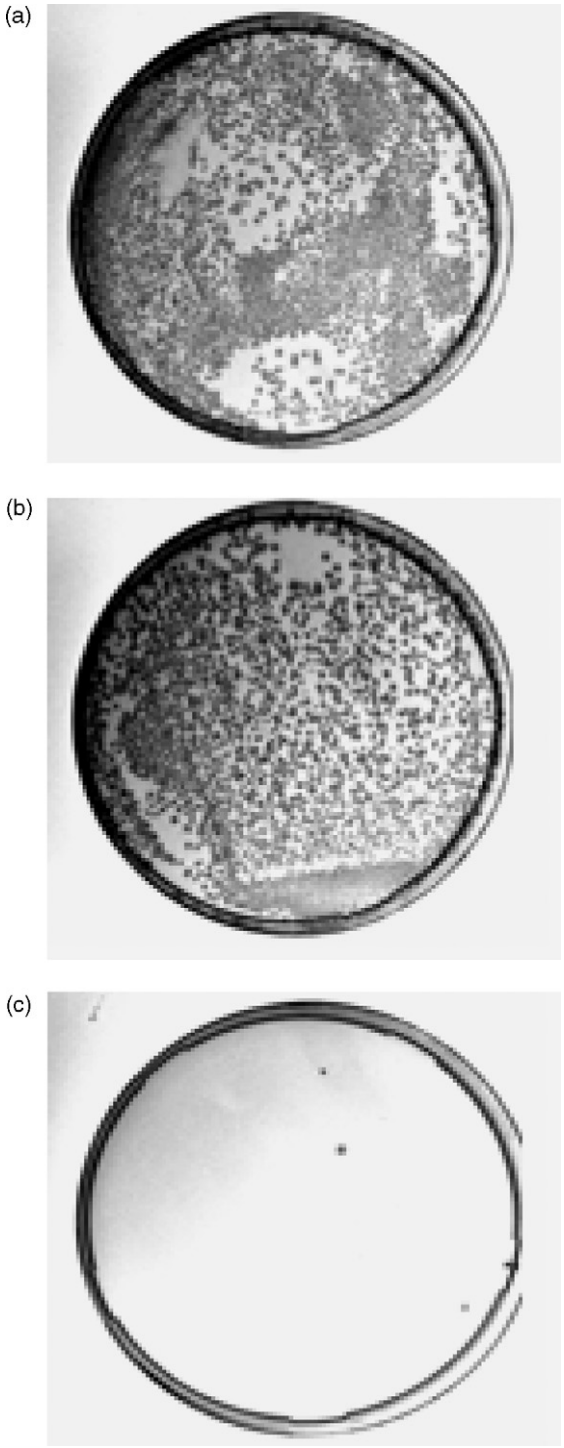

Fig. 10. Typical observations of Petri dishes after incubation of *E. coli* bacteria for 24 h at the surface of a control textile (a), a textile only impregnated with TiO_2 NPs (b), and a textile impregnated from an Ag–TiO_2 suspension (c).

for the growth and proliferation of different bacterial strains. On the other hand, they indicate that TiO_2 particles also allow the development of biological cells, which is in agreement with previous works performed in our laboratory showing the biocompatibility of sol–gel derived TiO_2 thin films [40]. Actually, it has been shown by other authors that TiO_2 NPs are not antibacterial in the absence of UV light [41]. In contrast, as illustrated in Fig. 10c, any cultivable bacteria could not be counted after 24 h of incubation on a textile impregnated from an Ag–TiO_2 suspension. Since TiO_2 NPs are not

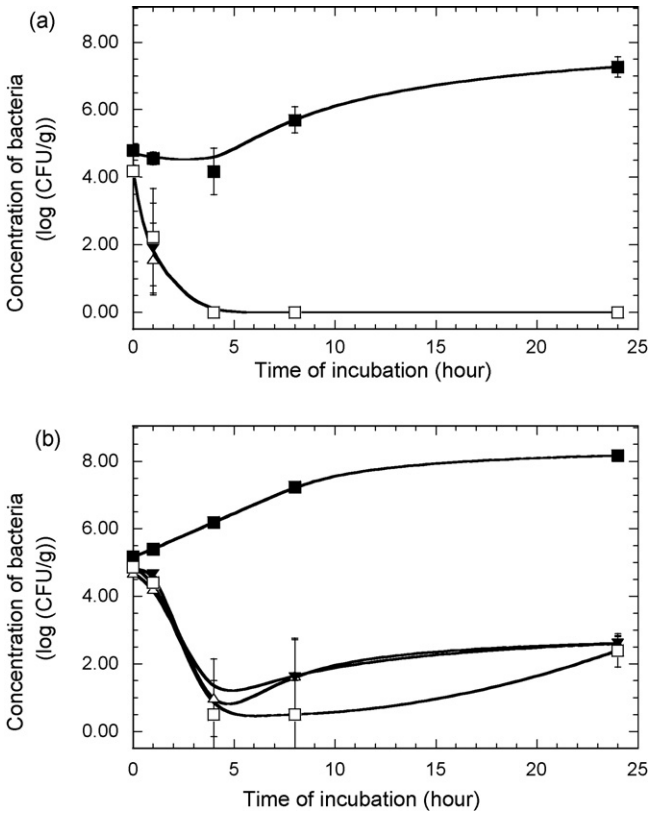

Fig. 11. Evolution kinetics of *E. coli* (a) and *L. innocua* bacteria (b) at the surface of a control textile (■), and textiles impregnated from Ag–TiO_2 suspensions, prepared as described in the text, and subsequently diluted in ethanol by a factor 1 (Δ), 5 (▼), and 10 (□).

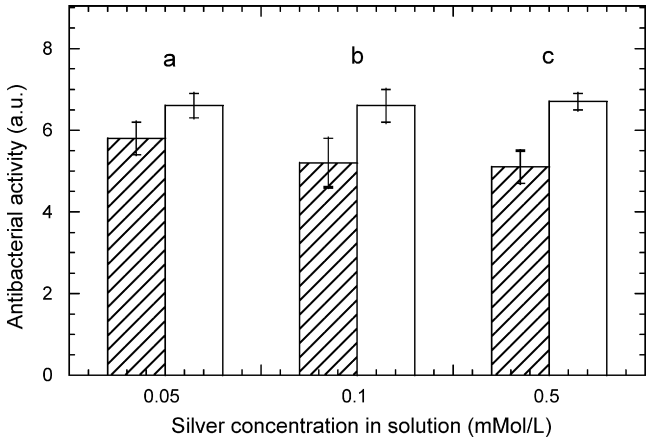

Fig. 12. Antibacterial activity against *L. innocua* (left) and *E. coli* (right), according to the ISO 20743/2005 standard, for textiles impregnated from Ag–TiO_2 suspensions, prepared as described in the text, and subsequently diluted in ethanol by a factor 10 (a), 5 (b), and 1 (c).

antibacterial in present experimental conditions, i.e. in the absence of UV light, Fig. 10c provides a first illustration of the antibacterial efficiency of textiles functionalized with Ag NPs.

This antibacterial efficiency was more precisely assessed by plotting log (CFU/g) as a function of the incubation time on various textile samples. Corresponding evolutions are illustrated in Fig. 11a and b for *E. coli* and *L. innocua* cells, respectively. Data illustrated in these figures first confirm that control textiles provide a good environment for bacterial growth. Both strains of bacteria are able to develop at the surface of textiles without Ag, which is depicted by an increasing number of colonies by approximately 2 log (CFU/g) after 24 h of incubation. In contrast, Fig. 11a and b clearly shows that Ag-treated textiles are effective against both bacteria. After a short incubation of 4 h, the number of both kinds of cells decreases by approximately 4 log (CFU/g). It means that the antibacterial effect of silver NPs is not restrained to a simple bacterial growth inhibition but effectively yields a nearly total mortality of bacterial cells. However, Fig. 11a and b also shows that further increase of the incubation duration induces some kinetic differences in relation to the bacteria nature. On the one hand, in the case of *E. coli*, quite no more viable bacteria are detected when increasing the incubation time from 4 to 24 h. On the other hand, for *L. innocua*, the number of cells gradually increases from a log (CFU/g) value of 0–1, reached after 4 h of incubation, to a log (CFU/g) value of about 2.5 after 24 h of incubation. It indicates a bi-regime evolution where (i) *L. innocua* bacteria are first efficiently, but not in their totality, killed at the contact of silver NPs, and (ii) a few surviving cells can develop again after a longer incubation time. Since silver particles do not continuously coat the textile fibres (Fig. 8b), it is inferred that some cells can eventually survive and undergo further development on textile areas poorly impregnated with silver, similarly to what is observed on a control textile. Besides, we have previously indicated that a majority of Ag NPs studied in this work exhibit diameters ranging from 2 to 15 nm. It has been shown that very small NPs can pass through the external wall of bacterial cells, i.e. break the peptidoglycan layer, and thereby destroy many Gram-positive and Gram-negative bacterial cells [42]. However, since the peptidoglycan layer in the former is substantially thicker than in the latter, Gram-positive bacteria are inferred to oppose an enhanced resistance to the antibacterial effects of active species. These remarks may explain some differences illustrated in Fig. 11a and b.

The most striking feature depicted in these figures, in presently studied conditions, is the absence of very significant influence of the impregnated silver amount on the antibacterial activity of functionalized textile fabrics. Indeed, Fig. 11a and b shows that, for both strains of studied bacteria, the impregnation of textile fabrics in suspensions, whose Ag concentration varies from 0.5×10^{-4} to 0.5×10^{-3} M, yields quite similar antibacterial kinetics. Influence of the impregnated silver amount has also been assessed through a quantification of the antibacterial activity according to the ISO 20743/2005 standard (see Section 2). Antibacterial activities are reported in Fig. 12 for functionalized textiles illustrated in Fig. 11a and b. Based on the standard definition, strong activities of 6.6 ± 0.4 and 5.5 ± 0.8 are deduced for *E. coli* and *L. innocua*, respectively, whatever the amounts of impregnated particles studied in this work. These data provide new illustration that (i) for fixed bacteria natures, a similarly strong antibacterial activity can be conferred to textile fabrics for a large range of impregnated silver amounts, and (ii) *L. innocua* can eventually oppose a stronger resistance than *E. coli* to the antibacterial activity induced by silver NPs.

3.8. Potential of our finished textiles: discussion

These studies firstly indicate the effectiveness of metallic silver NPs formed through our photocatalytic protocol. This result is in agreement with previous works devoted to the antibacterial functionalization of textile fabrics by plasma-deposited Ag NPs [26]. Generally speaking, the antibacterial activity of silver cations (silver salts or other silver compounds) and, more recently, that of silver nanoparticles, has been well established. Several studies propose that Ag NPs may attach to the surface of the cell membrane and disturb permeability and respiration functions of the cells. Smaller NPs having the larger surface area available for interaction would give more bactericidal effect than larger ones [43]. As already mentioned, it is possible that smallest Ag NPs not only interact with the surface of membrane, but can also penetrate inside the bac-

teria [12,42]. As established by the theory of hard/soft acids and bases, metallic silver particles are prone to react with phosphorus and sulphur compounds of the cell membrane [44,45]. In this hypothesis, interaction of Ag NPs with bacteria membranes is logically expected to depend on the active particle surface area, and smaller Ag particles are thus supposed to induce higher antibacterial activity than larger ones [46]. Another possibility to explain the antibacterial effect of metallic silver NPs would rely on the release of silver cations from nanoparticles, i.e. owing to their surface oxidation, such NPs would act as a tank of active silver cations [47]. According to the literature, the overall charge of bacteria at biological pH values is negative because of an excess number of carboxylic or other groups which, upon dissociation, make the cell surface electrically negative [48]. Hamouda and Baker have shown that the charge of antibacterial species can in turn be crucial for their activity [49].

Of course, the present work does not add to the knowledge in exact mechanisms involved in the antibacterial activity of metallic silver NPs, but it clearly reinforces the importance to study such NPs for antibacterial applications on textile fabrics. Our studies showed that a reduced quantity of impregnated Ag NPs was sufficient to confer a strong antibacterial activity to cotton-based textiles, and an excessive amount of antibacterial NPs did not add to this activity. This observation has an important consequence for practical applications. Due to plasmon effects, as illustrated in Fig. 3, an excessive amount of impregnated silver NPs can induce a brownish coloration of functionalized textiles. This feature is illustrated in Fig. 13c for a textile sample impregnated from a 0.5×10^{-3} M Ag suspension. The homogenous coloration shown in this figure provides an indication of the uniform distribution of silver NPs through textile fibres. However, such coloration generally appears to be an undesired event in practical applications. As shown in Fig. 13b, impregnation from a same suspension further diluted in ethanol by a factor 5 totally cancels coloration effects and allows preserving the visual aspect of a control textile (Fig. 13a). In the same time, data illustrated in Figs. 11 and 12 show that the absence of coloration induced by such a dilution does not reduce the antibacterial activity of impregnated textiles.

For practical uses of textile fabrics, it is generally required that finishing treatments exhibit sufficient fastness and strength in order to withstand friction damages and washing cycles. Fastness and strength of the finishing treatment in turn depend on the nature of bonds formed at the textile fibre surface, e.g. covalent bonding or physical attachment. In the present state, we are not in position to assess which kinds of bonds are formed at the fibre surface. However, a simple test already described in our previous paper [50] provided first insights in the fastness and strength of our finishing treatment. Textile samples were impregnated from an Ag–TiO_2 suspension, immersed in water, and then exposed to several ultrasonic agitation experimentations in a conventional ultrasound bath. The samples were then dried for 10 min at 110 °C, to remove water eventually impregnated within textile fibres during ultrasonication, and subsequently characterized through weight measurements and EDX analyses (not illustrated here). Weight measurements showed that, after 10 min of ultrasonification, the weight of impregnated matter was reduced by around 40% and did not evolve with further exposure to ultrasonic agitation. In the same time, EDX analyses indicated that the Ag/Ti atomic ratio was reduced by around 35% after a first ultrasound exposure of 10 min and did not evolve either with further exposure to ultrasounds. While we can still not conclude on the nature of bounds formed at the fibre surface, these results suggest that at least a part of Ag antibacterial species remain rather firmly bonded on textile fabrics. Of course, these tests do not account for true practical conditions and we cannot claim that, in the present state, our finishing treatment can withstand intensive friction damages or washing cycles, while preventing an unacceptable loss of antibacterial activity. These aspects should be the object of further specific investigations and eventual additional optimizations of our protocol.

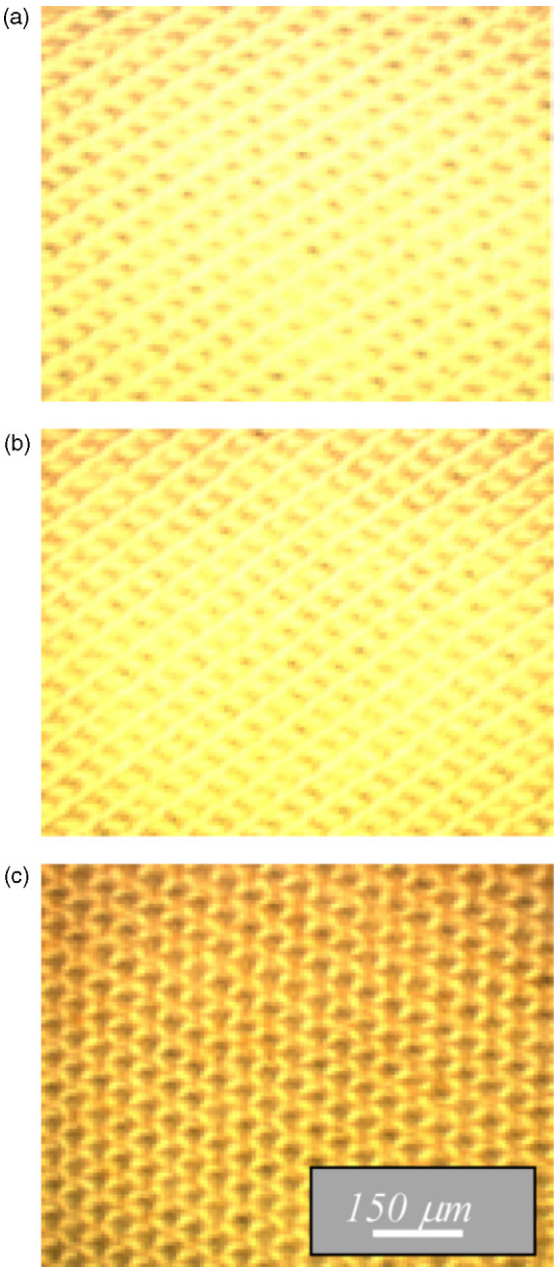

Fig. 13. Visual aspect of a control textile (a) and textiles impregnated from Ag–TiO_2 suspensions, prepared as described in the text, and subsequently diluted in ethanol by a factor 5 (b), and 1 (c). Scale bar is the same for all images.

4. Conclusion

An all-inorganic protocol, entirely based on wet chemistry methods, has been studied to form Ag NPs in solution. Liquid suspensions of anatase TiO_2 nanocrystallites have first been prepared through a sol–gel route. Silver NPs have then been generated through the photocatalytic reduction of silver nitrate diluted in TiO_2 liquid suspensions exposed to UV light, which results in the formation of a mixed Ag–TiO_2 suspension. UV/vis spectroscopy studies show that photo-metallization mechanisms leading to silver NPs are strongly influenced by the UV exposure duration in

relation to $AgNO_3$ and TiO_2 concentrations in solution. It is also shown that an excess of TiO_2 in the solution allows preventing fast decantation of so-formed Ag–TiO_2 liquid suspensions over post-metallization ageing, i.e. TiO_2 NPs in liquid suspensions not only act as photo-reductive reactants but also play a role of stabilizing agents. Chemico-structural and morphological characterizations of derived Ag particles demonstrate their metallic state, as well as their small size and rather narrow size distribution. Ag–TiO_2 suspensions have then been impregnated on cotton-based textile samples and the antibacterial activity of so-functionalized textiles has been studied with respect to *E. coli* and *L. innocua* bacteria. For both kinds of bacteria, functionalized textiles exhibit a strong antibacterial activity in a large range of impregnation conditions. It has been shown that TiO_2 particles, used to form Ag ones in solution, do not act in this antibacterial activity, which is entirely induced by photo-generated Ag NPs. Though, compared to *E. coli*, *L. innocua* exhibits in some extent a greater resistance to the antibacterial activity, these studies clearly demonstrate the effectiveness of silver NPs for antibacterial applications on textile samples. Besides, since this antibacterial activity is obtained even for reduced impregnated silver amounts, it has been possible to prevent any undesired textile coloration arising from silver NPs while keeping a strong activity of functionalized textiles. Further investigations are still needed to check how our impregnation protocol can allow withstanding friction damages and washing cycles for practical use applications.

Acknowledgements

This work was performed in the frame of the ACTIPROTEX research project supported by Techtera, the competitiveness cluster for technical and functional textiles based in the Rhône-Alpes Region in France, and by the French government (dgcis). The authors gratefully thank the Rhône-Alpes Region for financial support. They also thank partners from "Science et Surface" (Ecully, France) for their technical and scientific support in XPS measurements.

References

[1] B. Mahltig, D. Fiedler, H. Böttcher, J. Sol–Gel Sci. Technnol. 32 (2004) 219.
[2] I. Holme, Coloration Technol. 123 (2007) 59.
[3] B. Mahltig, H. Haufe, H. Böttcher, J. Mater. Chem. 15 (2005) 4385.
[4] R. Purwar, M. Joshi, AATCC Rev. 4 (2004) 22.
[5] P.K. Stoimenov, R.L. Klinger, G.L. Marchin, K.J. Klabunde, Langmuir 18 (2002) 6679.
[6] A.W. Bosman, H.M. Janssen, E.W. Meijer, Chem. Rev. 99 (1999) 1665.
[7] S.T. Dubas, P. Kumlangdudsana, P. Potiyaraj, Colloids Surf. A 289 (2006) 105.
[8] C. Yang, G. Liang, K. Xu, P. Gao, B. Xu, J. Mater. Sci. 44 (2009) 1894.
[9] J. Snouqiang, E. Newton, Y. Chun-Wah Marcus, K. Chi-Wai, Text. Res. J. 77 (2007) 85.
[10] P. Kulpinski, e-Polym. art.no.68 (2007).
[11] H.Y. Lee, H.K. Park, Y.M. Lee, K. Kim, S.B. Park, Chem. Commun. 15 (2007) 2959.
[12] J.R. Morones, J.L. Elechiguerra, A. Camacho, K. Holt, J.B. Kouri, J.T. Ramírez, M.J. Yacaman, Nanotechnology 16 (2005) 2346.
[13] M. Singh, S. Singh, S. Prasada, I.S. Gambhir, Dig. J. Nanomater. Bios. 3 (2008) 115.
[14] S.-H. Choi, Y.-P. Zhang, A. Gopalan, K.-P. Lee, H.-D. Kang, Colloids Surf. A 256 (2005) 165.
[15] T. Takeshi, W. Norihisa, T. Masaharu, Appl. Surf. Sci. 211 (2003) 189.
[16] C. Johans, J. Clohessy, S. Fantini, K. Kontturi, V.J. Cunnane, Electrochem. Commun. 4 (2002) 227.
[17] A. Taleb, C. Petit, M.P. Pileni, Chem. Mater. 9 (1997) 950.
[18] Z. Li, Y. Li, X.-F. Qian, J. Yin, Z.-K. Zhu, Appl. Surf. Sci. 250 (2005) 109.
[19] S. Eustis, M.A. El-Sayed, Chem. Soc. Rev. 35 (2006) 209.
[20] M. Brust, J. Fink, D. Bethell, D.J. Schiffri, C. Kiely, J. Chem. Soc. Chem. Commun. 16 (1995) 1655.
[21] J. Turkevich, P.C. Stevenson, J. Hillier, Discuss. Faraday Soc. 11 (1951) 55.
[22] M. Brust, M. Walker, D. Bethell, D.J. Schiffrin, R. Whyman, J. Chem. Soc. Chem. Commun. 7 (1994) 801.
[23] S. Pal, Y.K. Tak, J. Myong Song, Appl. Environ. Microbiol. 73 (2007) 1712.
[24] M. Burgos, M. Langlet, J. Sol–Gel Sci. Technol. 16 (1999) 267.
[25] M. Langlet, A. Kim, M. Audier, J. Mater. Sci. 38 (2003) 3945.
[26] E. Chadeau, N. Oulahal, L. Dubost, F. Favergeon, P. Degraeve, Food Control 21 (2010) 505.
[27] A. Wold, Chem. Mater. 5 (1993) 280.
[28] M. Langlet, A. Kim, M. Audier, C. Guillard, J.M. Herrmann, Thin Solid Films 429 (2003) 13.
[29] P.V. Kamat, J. Phys. Chem. B 106 (2002) 7729.
[30] A.L. González, C. Noguez, Comput. Theor. Nanosci. 4 (2007) 231.
[31] C. Sonnichsen, T. Franzl, T. Wilk, G.V. Plessen, J. Feldmann, New J. Phys. 4 (2002) 93.
[32] J.J. Mock, M. Barbic, D.R. Smith, D.A. Schultz, S. Schultz, J. Chem. Phys. 116 (2002) 6755.
[33] S.K. Ghosh, S. Kundu, M. Mandal, S. Nath, T. Pal, J. Nanoparticle Res. 5 (2003) 577.
[34] J. Kim, E. Kuk, K. Yu, J.O. Kim, S. Park, H. Lee, S. Kim, Y. Park, Y. Park, C. Hwang, Nanomed. Nanotechnol. 3 (2007) 95.
[35] A. Panáček, L. Kvítek, R. Prucek, M. Kolář, R. Veeřová, N. Pizúrová, V.K. Sharma, T. Nevěná, R. Zbořil, J. Phys. Chem. B 110 (2006) 16248.
[37] G. Schoen, Acta Chem. Scand. 27 (1973) 2623.
[38] S.W. Gaarenstroom, N. Winograd, J. Chem. Phys. 67 (1977) 3500.
[39] V.K. Kaushik, J. Electron Spectrosc. 56 (1991) 273.
[40] M. Manso, M. Langlet, M. Fernández, L. Vázquez, J.M. Martínez-Duart, Mater. Sci. Eng. C 23 (2003) 451.
[41] J.-Y. Choi, K.-H. Kim, K.-C. Choy, K.-T. Oh, K.-N. Kim, J. Biomed. Mater. Res. B Appl. Biomater. 80B (2007) 353.
[42] V.K. Sharma, R.A. Yngard, Y. Lin, Adv. Colloid Interf. Sci. 145 (2009) 83.
[43] L. Kvitek, A. Panaček, J. Soukupova, M. Kolar, R. Vecěrova, R. Prucek, M. Holecova, R. Zboril, J. Phys. Chem. C 112 (2008) 5825.
[44] D.W. Hatchett, H.S. White, J. Phys. Chem. 100 (1996) 9854.
[45] A. Sten, J. Chatt, N.R. Davies, Q. Rev. Chem. Soc. 12 (1958) 65.
[46] L. Chun-Nam, H. Chi-Ming, C. Rong, H. Qing-Yu, Y. Wing-Yiu, S. Hongzhe, T. Paul Kwong-Hang, C. Jen-Fu, C. Chi-Ming, J. Biol. Inorg. Chem. 12 (2007) 527.
[47] P.L. Taylor, O. Omotoso, J.B. Wiskel, D. Mitlin, R.E. Burrell, Biomaterials 26 (2005) 7230.
[48] S.M. Raffi, F. Hussain, T.M. Bhatti, J.I. Akhter, A. Hameed, M.M. Hasan, J. Mater. Sci. Technol. 24 (2008) 192.
[49] T. Hamouda, J.J. Baker, J. Appl. Microbiol. 89 (2000) 397.
[50] M. Messaoud, M. Houmard, S. Briche, F. Roussel, M. Langlet, J. Sol–gel Sci. Technol. (2010), first published on line, doi:10.1007/s10971-010-2240-7.